

A Double Machine Learning Trend Model for Citizen Science Data

Daniel Fink^{1*}, Alison Johnston², Matt Strimas-Mackey¹, Tom Auer¹, Wesley M. Hochachka¹, Shawn Ligocki¹, Lauren Oldham Jaromczyk¹, Orin Robinson¹, Chris Wood¹, Steve Kelling¹, and Amanda D. Rodewald¹

¹ Cornell Lab of Ornithology, Cornell University, Ithaca, NY 14850, USA.

² Centre for Research into Ecological and Environmental Modelling,
School of Maths and Statistics, University of St Andrews, St Andrews, UK.

* Corresponding author. daniel.fink@cornell.edu

Abstract

1. Citizen and community-science (CS) datasets have great potential for estimating interannual patterns of population change given the large volumes of data collected globally every year. Yet, the flexible protocols that enable many CS projects to collect large volumes of data typically lack the structure necessary to keep consistent sampling across years. This leads to interannual confounding, as changes to the observation process over time are confounded with changes in species population sizes.
2. Here we describe a novel modeling approach designed to estimate species population trends while controlling for the interannual confounding common in citizen science data. The approach is based on Double Machine Learning, a statistical framework that uses machine learning methods to estimate population change and the propensity scores used to adjust for confounding discovered in the data. Additionally, we develop a simulation method to identify and adjust for residual confounding missed by the propensity scores. Machine learning makes it possible to use large feature sets to control for confounding and model heterogeneity in trends. Using this new method, we can produce spatially detailed trend estimates from citizen science data.
3. To illustrate the approach, we estimated species trends using data from the CS project eBird. We used a simulation study to assess the ability of the method to estimate spatially varying trends in the face of real-world confounding. Results showed that the trend estimates distinguished between spatially constant and spatially varying trends at a 27km resolution. There were low error rates on the estimated direction of population change (increasing/decreasing) and high correlations on the estimated magnitude of population change.
4. The ability to estimate spatially explicit trends while accounting for confounding inherent in citizen science data has the potential to fill important information gaps, helping to estimate population trends for species and/or regions without rigorous monitoring data.

SECTION 1: Introduction

Information on population trends is essential for conservation monitoring and management. To date, the estimation of interannual trends has largely been restricted to the analysis of data from structured surveys where, ideally, the same observers follow the same survey protocols at the same locations, at same dates and times each year. This controlled survey structure is used to minimize the interannual variation in the observation process that can lead to confounding. This same structure also enables trends to be estimated using standard regression models (e.g. Kery & Royle, 2020; Link et al., 2020). However, these survey requirements have made it difficult to collect species-observation data at the scales necessary to monitor large groups of species across broad spatial extents, and at arbitrary times of year.

Citizen science projects are collecting increasingly large volumes of data for a variety of taxa (Pocock et al., 2017). The data collected by these projects have great potential to estimate population trends for species, regions, and times of year where structured data is lacking. However, one of the key challenges to using these data for trend estimation is controlling for confounding sources of interannual variation that lead to biased estimates (Bowler et al., 2022; Zhang et al., 2021).

Interannual change in surveying can arise from several sources and often many of these will act simultaneously. For example, studies have documented interannual variation in spatial site selection (August et al., 2020; Shirey et al., 2021; Zhang et al., 2021). Participant populations also change as new participants join projects and continuing participants improve the way they conduct surveys (Johnston et al., 2022). Improvements to equipment, such as binoculars, the development of species identification apps, and use of incentives or games (Xue et al., 2016) also can affect the observation process over time. In some cases, changes can be deliberate, as projects encourage certain survey protocols (e.g., submission of complete checklists; (Sullivan et al., 2009), whereas at other times unexpected events, such as the COVID pandemic, introduce interannual variation into citizen science observation processes (e.g. Hochachka et al., 2021).

Recent analytical developments in other fields have created an opportunity to use citizen science data for trend estimation whilst controlling for interannual confounding. Double Machine Learning (DML) is a statistical framework developed to utilize generic ML methods (e.g., random forests, lasso, penalized-regression, boosted models, deep neural networks) for causal inference (Chernozhukov et al., 2018). The DML framework was developed specifically to estimate heterogeneous treatment effects with large, feature-rich observational datasets, an important problem in many disciplines where confounding is a central concern, from economics (Athey, 2017) to personalized medicine (Obermeyer & Emanuel, 2016). Although DML can be used for causal inference, our goal here is focused on using DML to control for interannual confounding. End-users and practitioners must ultimately determine whether specific analyses can support causal inference, a distinction that requires application-specific assumptions.

When used to estimate population trends, the DML algorithm divides estimation into three separate prediction tasks. The goal of the first task is to estimate local species' population size averaged across the study period. To do this, a species distribution model is trained to learn how species observations vary with a set of features (e.g., climate, landcover, search effort). Machine learning methods are commonly used for species distribution modeling with large feature sets (e.g., Valavi et al., 2021; Waldo et al., 2022). The goal of the second task is to identify confounding in the data. To do this, a propensity score model is trained to learn how observation year systematically varies with the features (Ramsey et al., 2019). The ability to include large feature sets in the propensity model can be used to provide broad, detailed control for confounding. In the third task, the expected population size and observation year are used as benchmark values to help isolate the trend so it can be estimated without the influence of confounding features. In this third task, the inclusion of high-resolution spatial and environmental features creates the opportunity to generate spatially high-resolution trend estimates. The ability to capture trends with high (e.g. landscape scale) resolution is valuable for studying the processes affecting populations at these scales (e.g. agriculture, energy development, urbanization) (Rose et al., 2017).

In the DML framework outlined here, the propensity score model plays a critical role describing the patterns of interannual variation in sampling that can lead to confounding bias. It is therefore important to be able to quantify the degree to which this model adequately captures the interannual variation in sampling. To address this, we propose a novel simulation-based diagnostic tool to identify when the model fails to fully capture confounding sources of variation in the available data. When we identify residual confounding the diagnostic simulation can also be used to adjust the estimated population trends to account for this residual confounding.

We illustrate the real-world use of DML to estimate population trends using data from eBird, a popular citizen science project that has been collecting bird observation data since 2002 (Sullivan et al., 2014). eBird engages large numbers of participants who each decide where, when, and how to participate. Like many other citizen science projects, the limited structure in eBird has given rise to an evolving, heterogeneous observation process where interannual confounding is a central concern when estimating population trends. We estimated the average annual rate of change in breeding season abundance 2007–2019 at a 27km resolution across North America for wood thrush, Canada warbler, and long-billed curlew. This application presents the challenges of estimating trends with landscape-scale spatial resolution in the face of real-world confounding. We used a simulation study to assess the performance of the approach estimating the direction and magnitude of high-resolution trends while dealing with these challenges.

SECTION 2: The DML Trend Model

In this section, we introduce the DML trend model and the simulation-based diagnostic and adjustment for residual confounding. A simple motivating example is used to demonstrate how interannual confounding can be controlled using this approach.

SECTION 2.1 Double Machine Learning

To estimate interannual trends, we begin a model describing the variation in species abundance, which is called the outcome model,

$$Y = \tau Year + \mu(X) + \epsilon, \quad (1)$$

for which the objective is to estimate parameter τ , the effect of $Year$ on the reported abundance, Y . For convenience we assume Y is a real-valued measure of species abundance, but integer counts, or binary indicators of a species' occurrence can be accommodated without loss of generality. The function μ is a non-parametric function of the vector $X = (X_1, \dots, X_k)$ consisting of features that capture effects that are constant across years. Features in X can include both ecological process variables (e.g. habitat or climatic conditions) and observation process variables (e.g. search effort or time of day). The number of features, k , can be large.

The variable ϵ is a stochastic error term. If we assume X and $Year$ are the only features affecting abundance Y , and that X is uncorrelated with $Year$, then $E[\epsilon|X, Year] = 0$ and τ can therefore be estimated without bias. Confounding arises when there are other inter-annual changes in reported abundance that are not introduced by τ , for example if surveys are conducted in sites with better habitat quality over time. In such situations, employing estimation methods that do not account for the confounding can generate biased estimates of τ , because in the equation above all inter-annual changes are ascribed to τ (Imbens & Rubin, 2015).

A common strategy for obtaining unbiased estimates with confounding is to adjust estimation using propensity scores (Rosenbaum & Rubin, 1983). In this approach a propensity score model is introduced to keep track of confounding, which can be framed here as the dependence of $Year$ on features X . The propensity score model is written as,

$$Year = s(X) + \delta, \quad (2)$$

where s is a non-parametric function of the features X and δ is a stochastic error term where $E[\delta|X] = 0$. In general, there are no restrictions on the features used in the propensity score model. However, since the features associated with the reported abundance, X , have the potential to be confounders, it makes sense to include them in the propensity score model. Practically, it may be advantageous to include additional features or transformations of X to help model the dependence of $Year$.

DML solves equations (1) and (2) using an algorithm that decomposes trend estimation into three separate prediction tasks that can each be solved using generic machine learning methods (e.g. penalized-regression, lasso, random forests, boosted models, deep neural networks and ensembles

of these methods). In the first task, the marginal abundance is estimated (i.e. the abundance averaged across years). In the second task, the expected observation years are predicted based on the propensity model (2). In the third task these predictions are then plugged into a regression function that isolates the interannual variation in Y to estimate the trend τ . Importantly, the DML framework provides statistical guarantees establishing the convergence and asymptotic normality of the resulting estimator accounting for the fact that the plug-in values are themselves predictions (Chernozhukov et al., 2018). (See Supplemental Information for motivation of the DML estimator).

Here we used Causal Forests (Athey et al., 2019), which is an implementation of the DML framework that uses Random Forests (Breiman, 2001) as the machine learning model for each of the prediction tasks. By considering the trend τ to be a non-parametric function of vector $W = (W_1, \dots, W_m)$, the causal forests outcome model can be written:

$$Y = \tau(W)Year + \mu(X) + \epsilon. \quad (3)$$

The vector W , consists of features used to model heterogeneity in the trends and may overlap with X . The number of features, m , can be large. Note that this model can also be considered as a varying coefficient model for τ (Hastie & Tibshirani, 1993).

SECTION 2.2 Residual Confounding

Propensity score adjustments provide an effective strategy to control for interannual confounding provided the propensity score model $s(X)$ can sufficiently characterize the confounding in X . However, if $s(X)$ fails to fully capture the year-to-year variation associated with X , then there will be residual confounding. This situation can arise if X are well suited to explain patterns of marginal abundance $\mu(X)$ but not well suited to capture the interannual variation. For example, search duration, the amount of time spent searching for species, is often an important predictor of reported abundance. However, when participants decide how long they want to spend searching for species the duration can vary so widely that among-year changes in average search duration may not be detected in the propensity score model (Equation 2).

Here we present a simulation-based diagnostic and adjustment for residual confounding. First, a simulated dataset is constructed to have a known population trend while maintaining all the interannual confounding in X . Next, the DML trend estimate (including the propensity score adjustment) is computed from the simulated dataset. Differences between the known and estimated trend can be used to diagnose residual confounding bias. Critical to the success of the diagnostic and adjustment is that the simulated data realistically capture variation in reported abundance and confounding associated with X . We discuss the simulation construction for the motivating example in the next section and for the eBird analysis in Section 3.3.

SECTION 2.3 Motivating Example

We present a simple example to illustrate how the DML propensity score adjustment can control for the type of interannual confounding expected in many citizen science projects. To begin, we simulate a reported index of abundance generated according to the following process,

$$Y = 5h_1 + 5o_2 - 0.1Year + \epsilon,$$

where Y is the reported abundance on surveys, h is the amount of a habitat type in the survey area and positively associated with species abundance, o is the amount of search effort, and $\tau = -0.1$ is the per year rate of change in the abundance index (i.e. the population trend). Additionally, we create a confounding source of variation representing a trend in site selection where participants select sites with more habitat type h_1 in later years,

$$Year = h_1 + \delta.$$

We simulated 500 datasets and estimated the trend with and without the propensity score adjustment. Feature sets O & H were each independently sampled from $Uniform([-0.5, 0.5]^p)$ with $p = 25$ and sample size 1100, with 100 surveys each year from 2000 to 2010. The error terms were set to have a signal-to-noise ratio of 1, by sampling $\delta \sim N(0, \sigma_\delta)$ where σ_δ was specified such that

$sd(h)/\sigma_\delta = 1$ and $\epsilon \sim N(0, \sigma_\epsilon)$ where σ_ϵ was specified such that $sd(5h + 5o + Year)/\sigma_\epsilon = 1$. We used causal forests with the package *grf* (Tibshirani, et al. 2021) to estimate the population trend τ . These models included the following feature vectors $X = (h, o)$ for the marginal model, $X = (h)$ for the propensity score model, and $W = (w)$ for the trend model. To estimate the trend without the adjustment, we predicted $mean(Year)$ as a constant 'propensity score' for each year.

Our simulation used $\tau = -0.1$ which defines a declining population trend (Fig 1, blue lines). However, the increase in the surveying of the habitat type associated with higher species abundance, leads to upward trends in the reported species counts (Fig 1A). When no propensity score was used, the trend in site selection created spurious positive trends in abundance (Fig 1B, green lines). Including the propensity score adjustment reduced the bias of the estimated trend (Fig 1B, red lines), and the 95% confidence intervals covered the simulated trend of $\tau = -0.1$ in 90% of the 500 simulations.

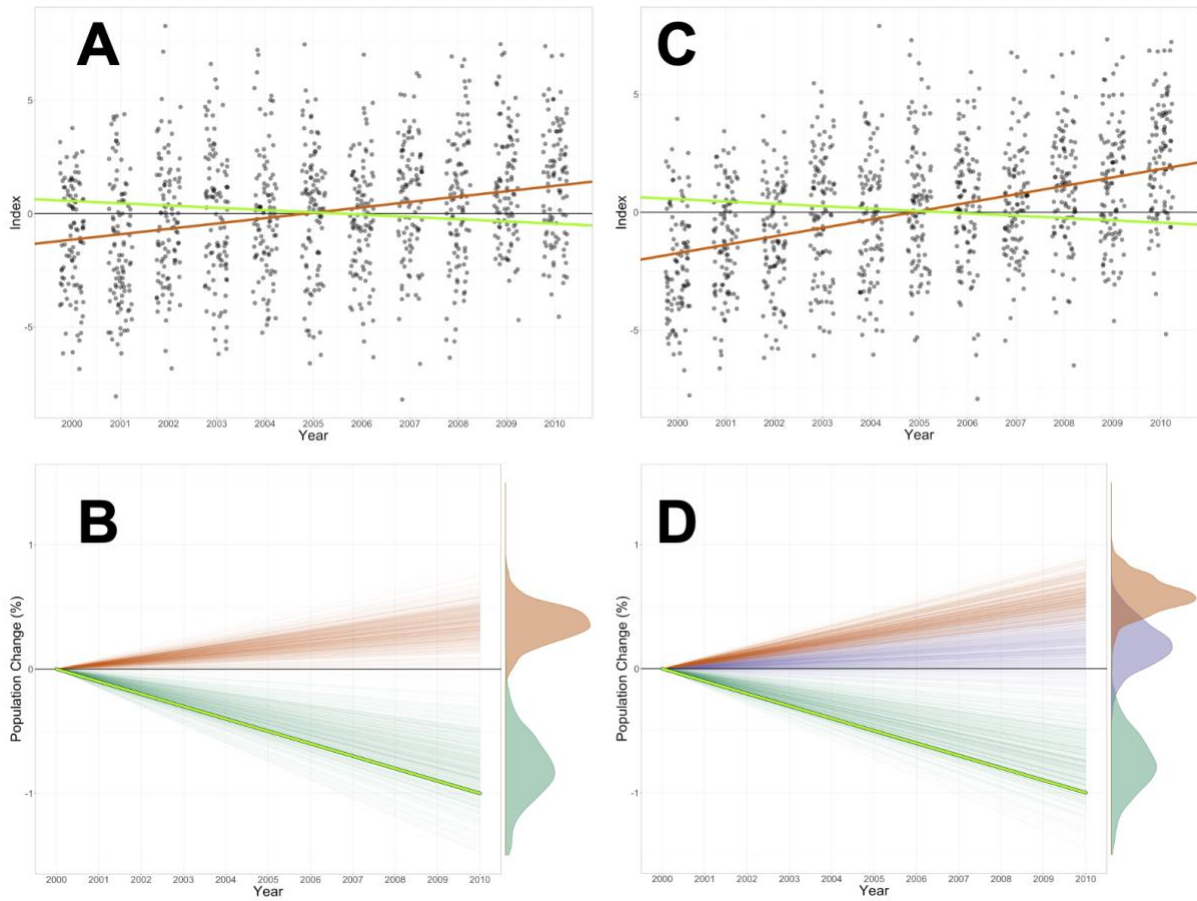


Figure 1: Motivating example. (A) Scatterplot of a single realization of simulated abundance data from 2000 -2010 with site selection confounding. The simulated trend (blue) and the trend fit with a simple linear regression (green). (B) Trajectories and marginal density plots of estimated trends without any adjustment (green), with the propensity score null-trend adjustment (orange). (C) Scatterplot of a single realization of simulated abundance data with site selection and search effort confounding. (D) Trajectories and marginal density plots of estimated trends without any adjustment (green), with propensity score adjustment (orange) and with the residual confounding adjustment (purple).

SECTION 2.4 Motivating Example with Residual Confounding

To illustrate the effects of residual confounding and the adjustment we included search effort o_2 as an additional confounding feature in the data generating process of the motivating example,

$$Year = h_1 + o_2 + \delta.$$

In addition to participants selecting sites with increasing amounts of habitat h in later years, they were also increasing the amount of effort o_2 spent searching for species. The feature vectors used to train the causal forests were $X = (h, o)$ for the marginal model, $X = (h)$ for the propensity score model, and $W = (w)$ for the trend model. By including only the habitat predictors h in X , the propensity score model could capture the interannual trend in site selection but the trend in search effort remained unmodelled.

Computing the residual confounding diagnostic required that we simulate datasets constructed to have a known population trends while maintaining all the interannual confounding in the original features (O, H, W) . A simple way to replicate the interannual variation in the original features is to resample them with replacement, stratified by year. Then the resampled features were used to generate simulated values of the reported abundance by applying the abundance process model with zero trend, $Y = 5h_1 + 5o_2 + \epsilon^*$.

The variance of ϵ and δ were scaled to maintain signal-to-noise ratios of one, and ϵ^* was sampled independently from $N(0, \sigma_\epsilon)$. All other data generation parameters for the motivating example were the same. We simulated 500 datasets and estimated the trend τ with three models:

- 1) Causal forests with the propensity score adjustment removed,
- 2) Casual forests with the propensity scores adjustment for the confounding of h_1 (but missing the unmodelled o_2 confounding), and
- 3) Causal forests with the propensity scores adjustment for the confounding of h_1 and additionally with the residual confounding adjustment with the synthetic data.

The confounding in this example generated a strong apparent positive trend among the reported abundance values even though the simulated trend was negative (Fig 1C). The propensity score adjustment reduced the bias of the estimated trend. Including the residual confounding adjustment provided enough control to reliably estimate the direction of the simulated trend. (Fig 1D). The 95% confidence intervals for the trend estimated with the residual confounding adjustment were not quite nominal and covered the true trend for 92% of the simulations.

SECTION 3: Trend Analysis of North American Breeding Birds

In this section we demonstrate how the proposed approach can be applied to estimate spatially explicit trends in abundance across large geographic extents with citizen science data. This application presents the real-world challenges of estimating spatially varying trends in the face of confounding based on temporally correlated species observations. A simulation study is used assess the performance of the propensity score adjustment, the trend and uncertainty estimates, and the ability to identify spatially structured trends. All computing was done in the R statistical computing language (R Core Team, 2019) and Causal Forests were fit using the *grf* package (Tibshirani et al., 2020) and were grown with 2000 trees using automatic parameter tuning for all parameters.

SECTION 3.1: Data

We estimated species trends using data from eBird, a popular citizen science project that has been collecting bird observation data since 2002 (Sullivan et al., 2014). eBird is a semi-structured survey (Kelling et al., 2019) because its flexibility allows participants to collect data in the ways they choose, but metadata are collected that describe the data collection methods. There are two important components of data collection that are followed by many eBird participants. First, participants are

encouraged to report all bird species detected and identified during the survey period, resulting in a *complete checklist* of bird species. This limits variation in preferential reporting rates across species and provides a basis to infer species non-detections. Second, participants are also encouraged to report characteristics of their birdwatching, for example the time of day and distance travelled. These variables and others can be used to adjust for variation in detection rates. The flexibility in protocol has given rise to an evolving, heterogeneous observation process where interannual confounding is a major concern when estimating population trends. This concern has compounded as eBird has continued to gain popularity engaging new communities of participants over the years.

We chose three species for which we will present trend estimates, selected to represent a range of different breeding niches, observation processes, and processes driving population change. Wood thrush (*Hylocichla mustelina*) is a commonly reported bird of the deciduous forest in eastern North America. Canada warblers (*Cardellina canadensis*) are a less commonly reported forest bird that breed in the boreal forest of North America. Long-billed curlew (*Numenius americanus*) is an infrequently reported shorebird that breeds in the grasslands of the Great Plains and Great Basin.

We used a subset of data from 2007 to 2019 within each species' previously identified breeding range and season (Fink, Auer, Johnston, Strimas-Mackey, et al., 2020) in which participants reported complete checklists of species counts for each survey. To prepare the data for the trend analysis we aggregated checklists using a (27km x 27km x 1week) grid based on checklist latitudes, longitudes, and dates. Four classes of variables were used in the trend models: (1) The total number of individuals of the given species reported in each grid cell was used as the reported outcome (Y), (2) Five observation effort features describing how participants conducted surveys were used to account for variation in detection rates, (3) Temporal features describing time of day and day of the year when surveys were conducted were used to account for variation in availability for detection, e.g. variation in behavior such as participation in the dawn chorus, (4) A suite of 66 spatial features describing the composition and configuration of landscapes in each grid cell were used to capture associations between species and elevation, topography, land & water cover, land use, hydrology, and road density. Please see the Supplemental Information for details about data and aggregation.

SECTION 3.2 Abundance model

Species expected abundance can be defined as the product of the species' occurrence rate, and the expected count of the species when it occurs within a given area and time window. Because interannual changes in species abundance can arise from changes in both the occurrence rate (e.g. as a function of whether the habitat is even suitable for a species) and changes in expected counts given occurrence, we adopted a hurdle model (Zuur et al., 2009) to explicitly capture changes in both processes. In the first stage we trained a DML model to estimate the interannual rate of change in occurrence rate based on the binary detection/non-detection of the species. In the second stage we trained another DML model to estimate the interannual rate of change in the log transformed count of individuals of the species based on the subset of surveys where the species was detected (i.e., all counts were positive). The average annual rate of change in species abundance was computed as the sum of the average annual rate of change in the occurrence rate and the average annual rate of change in species count given occurrence. For the feature sets in both models X included the (1) observation effort, (2) temporal, and (3) spatial features (including latitude and longitude to account for residual spatial patterns). To account for spatial variation in trends we included the spatial features in W .

We created an ensemble of the DML hurdle models by resampling data with replacement, thereby capturing sampling variation from both stages of the hurdle-model. Averaging the abundance trend estimates across the ensemble provided a simple way to control for overfitting (Efron, 2014). We calculated 80% confidence intervals using the lower 10th and upper 90th percentiles across the ensemble. Please see the Supplemental Information for additional information about constructing the ensemble.

SECTION 3.3: Simulation Construction

Simulations were used to diagnose the residual confounding and to evaluate the trend estimates. These simulations were constructed to meet four objectives: 1) To generate realistic patterns of each species' occurrence and counts on eBird checklists; 2) with specified trends in abundance; 3) a temporal correlation that arises from environmental stochasticity in population growth rates; and 4) replicating the interannual confounding in the eBird data. The following steps were used separately for each species to generate each species-specific simulated data set:

- 1) **Train generative model to learn species' occurrence and abundance.** We trained a predictive model (Fink, Auer, Johnston, Ruiz-Gutierrez, et al., 2020) to learn and then generate realistic patterns of variation in species' occurrence and counts on eBird checklists that were constant across years. To ensure that the generative model learned patterns constant across years it was trained using a random subset of the species' data with a permuted version of the observation year feature: $Year_p$. This model learned patterns for both the eBird observation process (e.g., variation in detection rates associated with varying amounts of search effort) and species ecological processes (e.g., variation in counts associated with environmental features).
- 2) **Generate simulated checklists, X^* .** To replicate the interannual variation in the original features X we generated the simulated checklists X^* by resampling the original features X with replacement, but in this step we stratified by year. The stratification by year ensures that any interannual changes in sampling are reflected in the simulated checklists X^* .
- 3) **Simulate species trends.** Using checklists X^* we initialized the simulated population for the first year of the study using the expected species occurrence rates and counts predicted from the generative model. Then population dynamics were simulated based on the permuted observation year feature, $Year_p$, using a discrete-time stochastic exponential growth model with a spatially explicit growth rate. Ten different simulation scenarios were created for each species with different patterns of population increase and decrease. The expected growth rates at each location were constant across years and varied according to the given simulation scenario. The ten simulation scenarios were generated, varying in direction, magnitude, and spatial patterns. Magnitudes were set to <1% (weak), 3.3% (moderate) and 6.7% per year (strong) based on IUCN Red List criteria (IUCN, 2019). The spatially varying trends were constructed to vary in direction and magnitude along a gradient from the core to the edge of the species' population (See Figure 2 and Figures SI-2 and SI-3). Finally, we included a stochastic component of the simulated growth rate to replicate the temporal correlation expected from interannual environmental stochasticity, an important characteristic of real species abundance data. The stochastic component varied independently among 27km grid cells and years with a standard deviation of approximately 6% per year.
- 4) **Simulate observations.** The observed checklist counts were simulated from the trajectories of expected population abundance created in step 3. The reported species detection was generated as a realization from a Bernoulli distribution based on the expected occurrence rate. Conditional on detection, we generated the reported checklist count as a realization from a Poisson distribution with rate set to be the logarithm of the expected count at each site in each year.

To maintain independence among the simulations used to train the residual confounding regression (See Section 3.4) and the simulations used to evaluate the trend estimates based on the regression adjustment, we used two entirely different sets of 5 scenarios for the training and evaluation tasks. Note that each set of scenarios contained comparable variation in trend direction, magnitude, and spatial patterns. Ten replicate datasets were generated for each of the scenarios. Please see the Supplemental Information for details about the generative model, simulation scenarios, and the discrete-time stochastic exponential growth model.

Section 3.4: Residual confounding

Interannual variation in how participants select sites, detect, identify, and count individuals generates distinct biases for each species. For this reason, we chose to implement the residual confounding diagnostics and adjustments at the species level, with the goal of finding an adjustment that would generalize well for all locations in the species range, regardless of the direction, magnitude, or spatial pattern of the unknown trend. To do this we fit a linear regression model for each species relating estimated trend values to simulated trend values across all locations within the species' range for all simulation scenarios. Then to adjust trend estimates for residual confounding, the regression was used to predict the expected trend based on the given estimate.

Section 3.5: Analysis workflow

We performed three simulation study analyses to assess the DML trend estimates followed by the trend estimates for each species.

SECTION 3.5.1: Propensity Score Performance

Our first analysis aimed at assessing the strength of the confounding bias in the eBird data and the performance of the propensity score adjustment. Using the simulated trends, we computed estimates with and without the propensity score adjustment. The species-level bias was assessed using the residual confounding regression (Section 3.4). The intercept parameter of the regression measured the distance between a zero-trend estimate and the corresponding expected value of the simulated trend. Thus, the intercept described the bias when estimating the trend direction (increasing or decreasing), with a value of zero indicating no *directional bias*. The slope parameter measured how simulated trends scaled with the direction and magnitude of the estimated trends, with a value of 1 indicating no *scaling bias*.

The parameter estimates are presented in Table 1. The slope parameters are negative indicating that estimates are greater than the expected simulated values, a positive directional bias. The propensity score adjustment reduced, though did not eliminate, this bias. The slope parameters were greater than 1 reflecting a general pattern of signal attenuation when estimating the trends (i.e., each percent increase in trend estimates was associated in less than a 1 percent increase in the expected simulated value). The propensity score adjustment decreased this attenuation for wood thrush and Canada warbler but did not significantly change it for long-billed curlew.

Species	Propensity Score Adjustment	Intercept	Intercept SE	Slope	Slope SE
Wood Thrush	No	-0.562	0.005	1.450	0.001
	Yes	-0.302	0.005	1.327	0.001
Canada Warbler	No	-2.009	0.011	1.557	0.002
	Yes	-0.859	0.010	1.424	0.002
Long-billed Curlew	No	-7.184	0.015	1.151	0.002
	Yes	-5.164	0.012	1.154	0.002

Table 1: Species-level estimates of confounding bias with and without propensity score adjustment. Slope and intercept estimates and standard errors (SE) are presented for each species.

SECTION 3.5.2: DML Trend estimate performance

Our second analysis assessed the performance of the DML trend estimates with the residual confounding adjustment. We evaluated the quality of the estimated trend magnitude (the average percent-per-year (PPY) rate of change in abundance 2007-19) and the trend direction (increasing/decreasing), two important inferential objectives for population monitoring. We determined that directional errors occurred when non-zero trends estimated the direction incorrectly. Non-zero trends were defined to occur when the 80% confidence interval did not contain zero. Therefore, we can consider directional errors to occur when trends were estimated to be significantly different from zero, but were in the opposite direction to the simulated trend. Because directional errors varied strongly with trend magnitude (Figure SI-1), we reported the mean directional error rate, binned into categories of trend magnitude (see Supplemental Information for more details about the directional error). We also computed Pearson's correlation between simulated and estimated trends for non-zero trend estimates. Finally, we assessed the coverage of the resampling-based uncertainty estimates as the percentage of all 27km locations where the estimated intervals contained the simulated trend value.

The mean directional error rate among non-zero trends was low for all species (Table 2). The correlations among non-zero estimates and simulated values was high. As expected, the directional error rates increased and the correlations decreased with the volume of species' data that were non-zero counts; from wood thrush (a commonly reported species in a region with high data density), to Canada warbler (less commonly reported in regions with less data density), to long-billed curlew (infrequently reported compared to Wood Thrush and Canada Warbler within a relatively low data density region of the continent). Interval coverage increased with decreasing amounts of species data, though it was markedly less than the nominal confidence 80% level for all species.




Species		Trend Scenarios	Directional Error	Correlation	CI Coverage
 Wood Thrush <i>Hylocichla ustulata</i>	Wood Thrush	All	2.5%	95%	46%
		Constant	1.8%	90%	49%
		Varying	1.7%	96%	41%
 Canada Warbler <i>Cardellina canadensis</i>	Canada Warbler	All	4.2%	87%	53%
		Constant	3.1%	82%	56%
		Varying	4.1%	93%	49%
 Long-billed Curlew <i>Numenius americanus</i>	Long-billed Curlew	All	4.6%	84%	58%
		Constant	5.6%	83%	62%
		Varying	3.3%	90%	53%

Table 2: Trend estimate performance. The directional error, correlation, and interval coverage are presented for each species, averaged across all evaluation scenarios (All) the spatially constant evaluation scenarios (Constant), across the spatially varying scenarios (Varying).

SECTION 3.5.3: Performance identifying spatial trends

Our third analysis assessed model performance identifying spatial heterogeneity in trends. We compared model performance between spatially constant and spatially varying scenarios for each species (Table 2). The similarity in performance between constant and varying trends highlights the ability of the model to adapt to heterogeneous trends. Figure 2 shows trend maps for Wood Thrush for a single realization of the simulation scenarios (See Supplemental Materials Figures SI1 & SI2 for Canada warbler and long-billed curlew). These maps show how the model adapted to simulations with different directions, magnitudes, and spatial patterns.

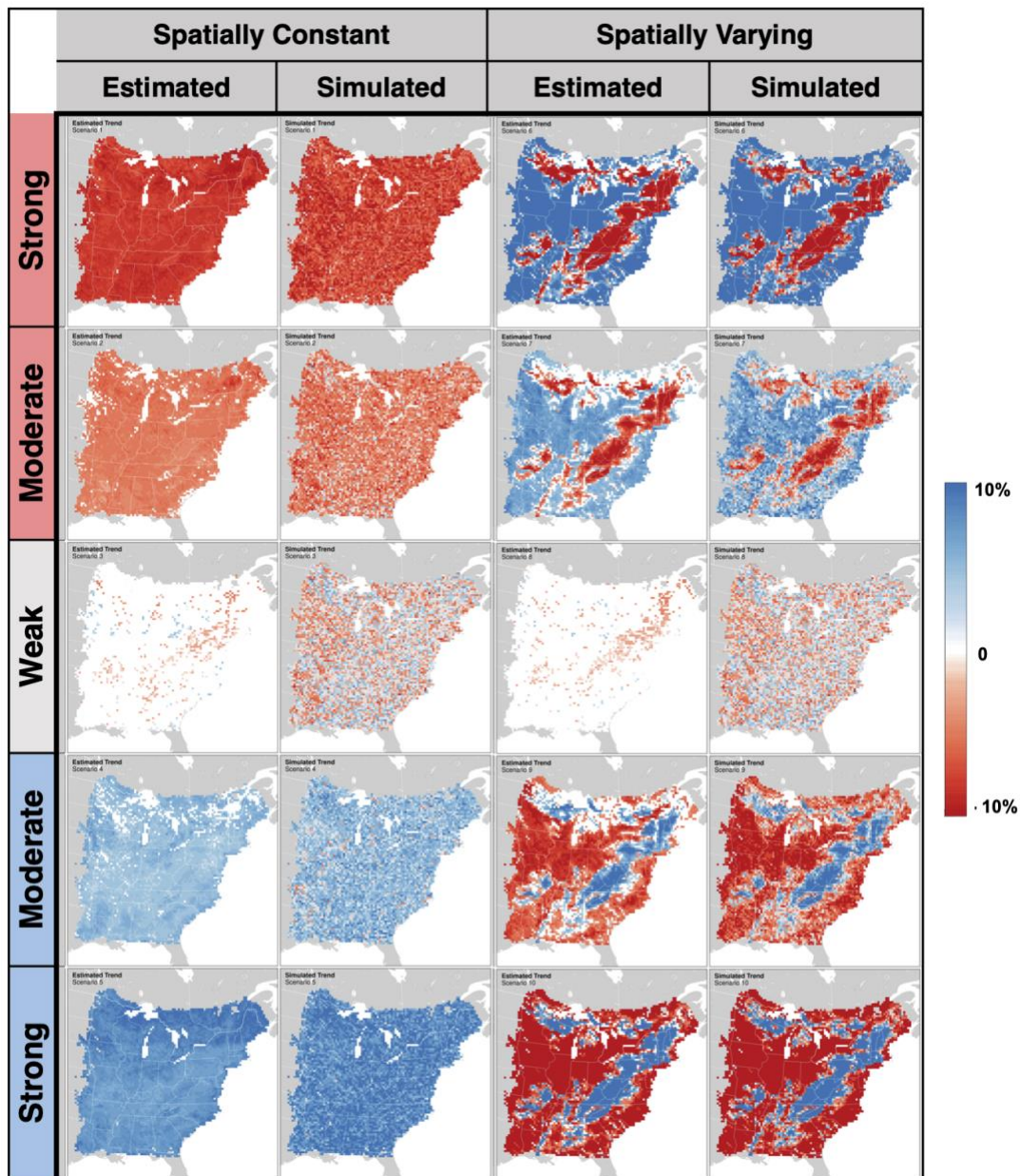


Figure 2: Wood Thrush Trend Simulations. All trend maps show the average annual percent-per-year change in abundance from 2007–2019 within 27km pixels (red=decline, blue=increase, white=80% confidence interval contained zero), intensity (darker colors indicate stronger trends). Simulated trends show scenarios varying by direction and magnitude along rows: weak (includes trends $\sim|1\%/yr|$), moderate (includes regions with trends $\sim|3.5\%/yr|$), and strong trends (includes regions with trends $\sim|6.7\%/yr|$). The columns show simulated and estimated trends for spatially constant and varying simulation scenarios.

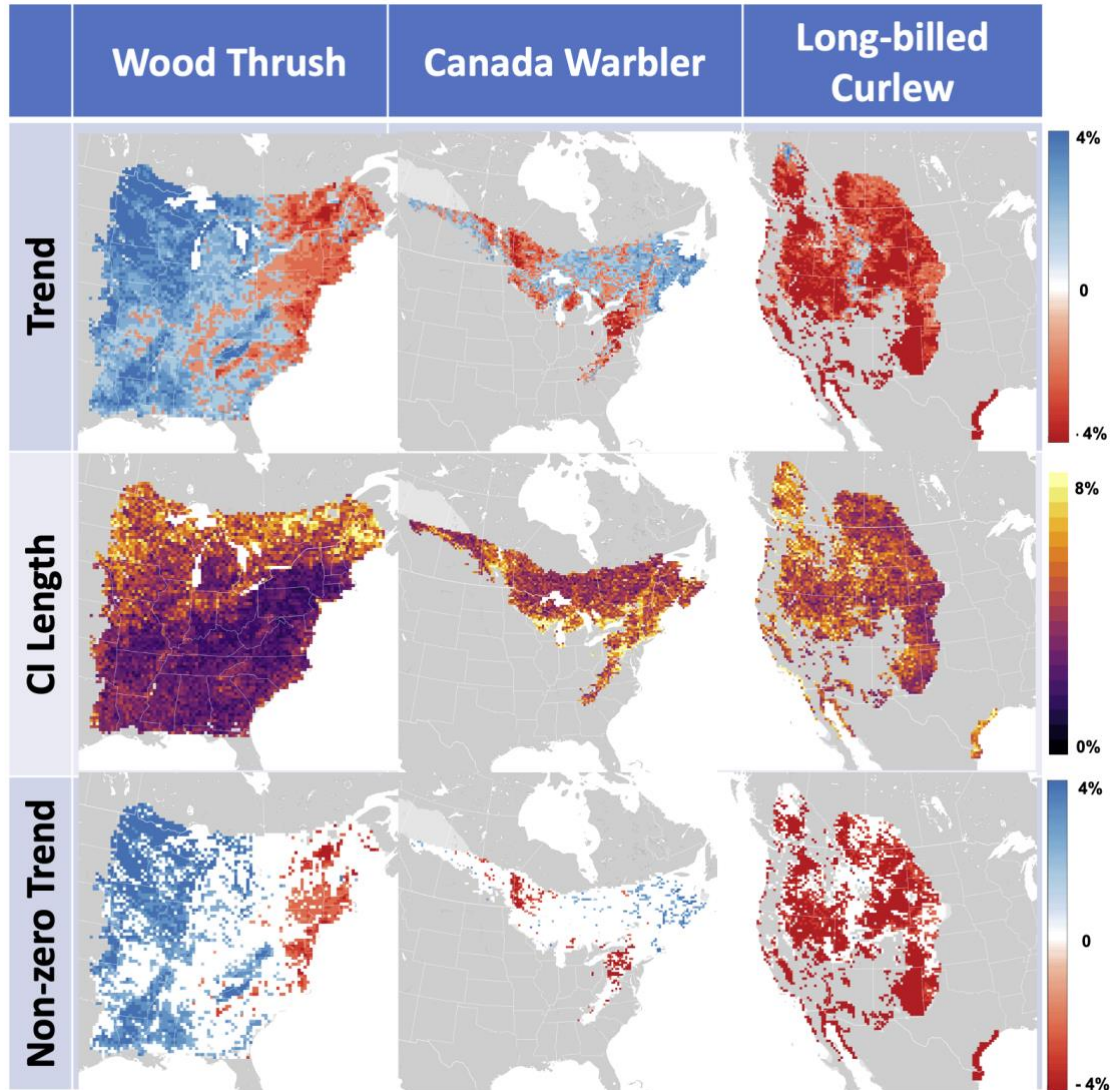


Figure 3: Trend estimates Wood Thrush, Canada Warbler and Long-billed Curlew. All trend maps show the average annual percent-per-year change in abundance from 2007–2019 within 27km pixels (red=decline, blue=increase), intensity (darker colors indicate stronger trends). The top row shows the estimated trends, middle row shows confidence interval length, and the bottom panel shows the non-zero trends in red and blue with white in locations where 80% confidence interval contained zero.

SECTION 3.5.4: Species trends

Figure 3 shows maps of average annual percent-per-year change in abundance from 2007–2019 for all three species. The Wood Thrush population shows steep declines in the northeast and increases in the southwest of its breeding season population, a pattern similar to other published studies (e.g. Fink, Auer, Johnston, Ruiz-Gutierrez, et al., 2020). The estimated population change for Canada Warbler also shows spatial patterning, though the uncertainty is relatively high. Long-billed Curlew shows strong, significant range-wide declines consistent with previous analysis (Rosenberg et al., 2019).

SECTION 4: DISCUSSION

Section 4.1: Confounding in CS data

Estimating the interannual rate of population change using unstructured or semi-structured citizen science data is a difficult task because of the inherent risk of confounding. The analyses of eBird data presented here showed that confounding bias can be strong (7% directional bias for long-billed curlew), though it varied among species (0.6% directional bias for wood thrush). The simulation study showed that the propensity score adjustment used in the DML framework reduced, though did not completely remove, the eBird confounding bias. With the simulation-based residual confounding adjustment, the method performed well distinguishing between spatially constant and spatially varying patterns at a 27km×27km resolution and produced estimates that had a high degree of consistency with trend direction and magnitude across multiple simulation scenarios.

These results indicate the potential of the method to deliver useful trend information in real-world analysis of citizen science data. Further research will be needed to understand the full potential and limitations of the approaches presented here. This includes the analysis of other data sets, with different taxa, across different spatial and temporal extents and scales. In applications that seek to study large spatial extents with high resolution, nonstationary trend effects may become a challenge as the processes driving population change are more like to vary across broad extents (Rose et al., 2017). Identifying shared biases across analyses can also provide information about the observation process. The positive directional bias shared among the three study species is consistent with participants learning how to select better survey sites and how to better detect, identify, and count species with experience (Johnston et al., 2022; Kelling et al., 2015) though analysis of additional species would be needed to test this hypothesis.

It is important to recognize that neither the propensity score adjustment nor the simulation-based residual confounding adjustment can control for confounders that are missing from the analysis and independent of X , the features in hand. Asserting the absence of *hidden confounders*, as they are known in the causal inference literature, is a key assumption required to draw causal inferences from regression models like DML (Imbens & Rubin, 2015) and often requires strong analysis-specific assumptions. This limitation suggests a general modelling strategy that leverages the machine learning part of DML to minimize confounding bias and guard against hidden confounding by including features describing *all* possible sources of variation in the propensity scores and the abundance outcomes.

Section 4.3: Estimating Uncertainty

Estimating uncertainty for the eBird analysis presented two challenges that were not present in the simplistic motivating example. The first challenge was to capture the sampling variation from both steps of the trend hurdle model. To do this we used a resampling approach to propagate uncertainty from both estimation steps when estimating the 80% intervals. The second challenge was to assess the DML performance estimating uncertainty based on temporally correlated counts. This challenge was important because the DML outcome model did not include structure or features to account for temporal correlation, a common feature of species count data.

The simulation results showed that coverage for the eBird analysis was well below the nominal 80% level. We believe that this is, at least in part, because the outcome model is not accounting for the temporal correlation. Interestingly, the simulation results showed that there was strong directional error control when interval estimates were used to identify non-zero trends, i.e., estimates whose intervals did not contain zero. This suggests that the uncertainty may not be scaling appropriately with the magnitude of the trend. Accounting for temporal correlation in the outcome is an interesting direction for further research into the DML framework. Incorporating more powerful rules to identify non-zero trends that control for multiple comparisons and spatial correlation (e.g. false detection rate

thresholding) could also serve to improve the power of the approach and scope of inference for species with weaker trend signals like Canada warbler.

Section 4.4: Generalizations

The DML trend model and the simulation-based adjustment presented here can be used with a variety of data types and applications. The causal forest implementation used in this paper can accommodate binary and real valued outcome variables, making it possible to estimate trends in species occurrence rates, expected trends, and other indices of abundance.

For the eBird analysis presented here we utilized the fact that outcome variable, counts, were collected as part of a complete checklist of species reported within some taxonomic group to infer the zero counts associated with non-detection. The same approach can be used with other checklist-based citizen science projects to analyse counts as well as binary response presence-absence data (e.g. birds BTO 2017; Swiss bird project; and butterflies van Swaay et al., 2008). Even when observations are not collected in the form of complete lists, (Henckel et al., 2020; van Strien et al., 2013) demonstrated that observations can, at least for some taxa, be assembled into checklists making them amenable to DML trend analysis. It may also be possible to analyse presence-only data (e.g. iNaturalist.org) by carefully selecting (Valavi et al., 2021) or weighting (Fithian & Hastie, 2013) background data. However, more research will be needed to carefully consider biases and confounding associated when presence-only data (e.g. Stoudt et al., 2022). The DML trend model may even be useful for the analysis of data collected from structured surveys where confounding can arise despite survey structure. For example, Zhang et al. (2021) describe how changes in habitat were confounded with reporting biases for the North American BBS, a survey that uses repeated interannual visits to control for sources of confounding.

SECTION 5: Conclusion

eBird exemplifies the risks of interannual confounding common to many citizen projects as participants and modes of participation have changed over time. Fostering opportunities for citizen participants to learn about nature and engage with like-minded communities are important goals for many of these projects. However, these goals naturally lead to changes in how participants collect data making interannual confounding an inherent risk using data for these programs. Continued research to identify sources of interannual confounding among citizen science projects will be valuable for future efforts estimating trends especially for integrating data from different programs.

The volume of citizen science data is rapidly growing, but the lack of structured protocols has rendered most of these data unsuitable for estimating population trends. Bias can be introduced by changes over time in how people participate. The DLM trend model presented here can account for these confounding changes over time. When used appropriately, including assessments of the propensity score model to account for sources of confounding variation, this approach has the potential to increase the biodiversity monitoring value that we can obtain from citizen data. This could enable us to better track population changes in areas of the world with fewer structured monitoring programmes.

Acknowledgments: The eBird and the eBird Status and Trends projects rely on the time, and dedication and support from countless individuals and organizations. We thank the many thousands of eBird participants for their contributions and the eBird team for their support.

Funding: This work was funded by The Leon Levy Foundation, The Wolf Creek Foundation, and the National Science Foundation (ABI sustaining: DBI-1939187). This work used Bridges2 at Pittsburgh Supercomputing Center and Anvil at Rosen Center for Advanced Computing at Purdue University through allocation DEB200010 from the Advanced Cyberinfrastructure Coordination Ecosystem: Services & Support (ACCESS) program, which is supported by National Science Foundation grants #2138259, #2138286, #2138307, #2137603, and #2138296. Our research was also funded through

the 2017-2018 Belmont Forum and BiodivERsA joint call for research proposals, under the BiodivScen ERA-Net COFUND program, with financial support from the Academy of Finland (AKA, Univ. Turku: 326327, Univ. Helsinki: 326338), the Swedish Research Council (Formas, SLU: 2018-02440, Lund Univ.: 2018-02441), the Research Council of Norway (Forskningsrådet, NINA: 295767) and the U.S. National Science Foundation (NSF, Cornell Univ.: ICER-1927646).

Data availability: All bird observation data used to conduct this study are publicly available on the eBird website <https://ebird.org/science/use-ebird-data>. All environmental data used to conduct this study are publicly available. See Supplemental Information and Table SI-1 for references and links. To maintain the privacy of eBird participants' personally identifiable information the Checklist Calibration Index data (see Supplemental Information) cannot be made publicly available.

References

- Athey, S. (2017). Beyond prediction: Using big data for policy problems. *Science*, 355(6324), 483–485. <https://doi.org/10.1126/science.aal4321>
- Athey, S., Tibshirani, J., & Wager, S. (2019). Generalized random forests. *The Annals of Statistics*, 47(2), 1148–1178.
- August, T., Fox, R., Roy, D. B., & Pocock, M. J. O. (2020). Data-derived metrics describing the behaviour of field-based citizen scientists provide insights for project design and modelling bias. *Scientific Reports*, 10(1), 11009. <https://doi.org/10.1038/s41598-020-67658-3>
- Bowler, D. E., Callaghan, C. T., Bhandari, N., Henle, K., Benjamin Barth, M., Koppitz, C., Klenke, R., Winter, M., Jansen, F., Bruelheide, H., & Bonn, A. (2022). Temporal trends in the spatial bias of species occurrence records. *Ecography*. <https://doi.org/10.1111/ecog.06219>
- Breiman, L. (2001). Random forests. *Machine Learning*, 45(1), 5–32.
- Chernozhukov, V., Chetverikov, D., Demirer, M., Duflo, E., Hansen, C., Newey, W., & Robins, J. (2018). Double/debiased machine learning for treatment and structural parameters. *The Econometrics Journal*, 21(1), C1–C68. <https://doi.org/10.1111/ectj.12097>
- Efron, B. (2014). Estimation and Accuracy After Model Selection. *Journal of the American Statistical Association*, 109(507), 991–1007. <https://doi.org/10.1080/01621459.2013.823775>
- Fink, D., Auer, T., Johnston, A., Ruiz-Gutierrez, V., Hochachka, W. M., & Kelling, S. (2020). Modeling avian full annual cycle distribution and population trends with citizen science data. *Ecological Applications*, 30(3), e02056.
- Fink, D., Auer, T., Johnston, A., Strimas-Mackey, M., Robinson, O., Ligoeki, S., Hochachka, W., Wood, C., Davies, I., & Iliff, M. (2020). *EBird Status and Trends, Data Version: 2019; Released: 2020. Cornell Lab of Ornithology, Ithaca, New York*.
- Fithian, W., & Hastie, T. (2013). Finite-Sample Equivalence in Statistical Models for Presence-Only Data. *The Annals of Applied Statistics*, 7(4), 1917–1939. <https://doi.org/10.1214/13-AOAS667>
- Hastie, T., & Tibshirani, R. (1993). Varying-Coefficient Models. *Journal of the Royal Statistical Society: Series B (Methodological)*, 55(4), 757–779. <https://doi.org/10.1111/j.2517-6161.1993.tb01939.x>
- Henckel, L., Bradter, U., Jönsson, M., Isaac, N. J. B., & Snäll, T. (2020). Assessing the usefulness of citizen science data for habitat suitability modelling: Opportunistic reporting versus sampling based on a systematic protocol. *Diversity and Distributions*, 26(10), 1276–1290. <https://doi.org/10.1111/ddi.13128>
- Hochachka, W. M., Alonso, H., Gutiérrez-Expósito, C., Miller, E., & Johnston, A. (2021). Regional variation in the impacts of the COVID-19 pandemic on the quantity and quality of data collected by the project eBird. *Biological Conservation*, 254, 108974. <https://doi.org/10.1016/j.biocon.2021.108974>
- Imbens, G. W., & Rubin, D. B. (2015). *Causal inference in statistics, social, and biomedical sciences*. Cambridge University Press.
- IUCN. (2019). *The IUCN Red List of Threatened Species. Version 2019*. <https://www.iucnredlist.org>

- Johnston, A., Matechou, E., & Dennis, E. B. (2022). Outstanding challenges and future directions for biodiversity monitoring using citizen science data. *Methods in Ecology and Evolution*, n/a(n/a). <https://doi.org/10.1111/2041-210X.13834>
- Kelling, S., Johnston, A., Bonn, A., Fink, D., Ruiz-Gutierrez, V., Bonney, R., Fernandez, M., Hochachka, W. M., Julliard, R., Kraemer, R., & Guralnick, R. (2019). Using Semistructured Surveys to Improve Citizen Science Data for Monitoring Biodiversity. *BioScience*, 69(3), 170–179. <https://doi.org/10.1093/biosci/biz010>
- Kelling, S., Johnston, A., Hochachka, W. M., Iliff, M., Fink, D., Gerbracht, J., Lagoze, C., Sorte, F. A. L., Moore, T., Wiggins, A., Wong, W.-K., Wood, C., & Yu, J. (2015). Can Observation Skills of Citizen Scientists Be Estimated Using Species Accumulation Curves? *PLOS ONE*, 10(10), e0139600. <https://doi.org/10.1371/journal.pone.0139600>
- Kery, M., & Royle, J. A. (2020). *Applied Hierarchical Modeling in Ecology: Analysis of Distribution, Abundance and Species Richness in R and BUGS: Volume 2: Dynamic and Advanced Models*. Academic Press.
- Link, W. A., Sauer, J. R., & Niven, D. K. (2020). Model selection for the North American Breeding Bird Survey. *Ecological Applications*, 30(6), e02137. <https://doi.org/10.1002/eap.2137>
- Obermeyer, Z., & Emanuel, E. J. (2016). Predicting the Future—Big Data, Machine Learning, and Clinical Medicine. *The New England Journal of Medicine*, 375(13), 1216–1219. <https://doi.org/10.1056/NEJMp1606181>
- Pocock, M. J. O., Tweddle, J. C., Savage, J., Robinson, L. D., & Roy, H. E. (2017). The diversity and evolution of ecological and environmental citizen science. *PLOS ONE*, 12(4), e0172579. <https://doi.org/10.1371/journal.pone.0172579>
- R Core Team. (2019). *R: A Language and Environment for Statistical Computing*. R Foundation for Statistical Computing. <https://www.R-project.org/>
- Ramsey, D. S. L., Forsyth, David. M., Wright, E., McKay, M., & Westbrooke, I. (2019). Using propensity scores for causal inference in ecology: Options, considerations, and a case study. *Methods in Ecology and Evolution*, 10(3), 320–331. <https://doi.org/10.1111/2041-210X.13111>
- Rose, K. C., Graves, R. A., Hansen, W. D., Harvey, B. J., Qiu, J., Wood, S. A., Ziter, C., & Turner, M. G. (2017). Historical foundations and future directions in macrosystems ecology. *Ecology Letters*, 20(2), 147–157.
- Rosenbaum, P. R., & Rubin, D. B. (1983). The central role of the propensity score in observational studies for causal effects. *Biometrika*, 70(1), 41–55.
- Rosenberg, K. V., Dokter, A. M., Blancher, P. J., Sauer, J. R., Smith, A. C., Smith, P. A., Stanton, J. C., Panjabi, A., Helft, L., & Parr, M. (2019). Decline of the North American avifauna. *Science*, 366(6461), 120–124.
- Shirey, V., Belitz, M. W., Barve, V., & Guralnick, R. (2021). A complete inventory of North American butterfly occurrence data: Narrowing data gaps, but increasing bias. *Ecography*, 44(4), 537–547. <https://doi.org/10.1111/ecog.05396>
- Stoudt, S., Goldstein, B. R., & de Valpine, P. (2022). Identifying engaging bird species and traits with community science observations. *Proceedings of the National Academy of Sciences*, 119(16), e2110156119.
- Sullivan, B. L., Aycrigg, J. L., Barry, J. H., Bonney, R. E., Bruns, N., Cooper, C. B., Damoulas, T., Dhondt, A. A., Dietterich, T., & Farnsworth, A. (2014). The eBird enterprise: An integrated approach to development and application of citizen science. *Biological Conservation*, 169, 31–40.
- Sullivan, B. L., Wood, C. L., Iliff, M. J., Bonney, R. E., Fink, D., & Kelling, S. (2009). eBird: A citizen-based bird observation network in the biological sciences. *Biological Conservation*, 142(10), 2282–2292.
- Tibshirani, J., Athey, S., & Wager, S. (2020). *Grf: Generalized Random Forests*. R package version 120.
- Valavi, R., Elith, J., Lahoz-Monfort, J. J., & Guillera-Arroita, G. (2021). Modelling species presence-only data with random forests. *Ecography*, 44(12), 1731–1742.

- van Strien, A. J., van Swaay, C. A. M., & Termaat, T. (2013). Opportunistic citizen science data of animal species produce reliable estimates of distribution trends if analysed with occupancy models. *Journal of Applied Ecology*, 50(6), 1450–1458. <https://doi.org/10.1111/1365-2664.12158>
- van Swaay, C. A. M., Nowicki, P., Settele, J., & van Strien, A. J. (2008). Butterfly monitoring in Europe: Methods, applications and perspectives. *Biodiversity and Conservation*, 17(14), 3455–3469. <https://doi.org/10.1007/s10531-008-9491-4>
- Waldock, C., Stuart-Smith, R. D., Albouy, C., Cheung, W. W. L., Edgar, G. J., Mouillot, D., Tjiputra, J., & Pellissier, L. (2022). A quantitative review of abundance-based species distribution models. *Ecography*, 2022(1). <https://doi.org/10.1111/ecog.05694>
- Xue, Y., Davies, I., Fink, D., Wood, C., & Gomes, C. P. (2016). *Avicaching: A Two Stage Game for Bias Reduction in Citizen Science*. 10.
- Zhang, W., Sheldon, B. C., Grenyer, R., & Gaston, K. J. (2021). Habitat change and biased sampling influence estimation of diversity trends. *Current Biology*, 31(16), 3656–3662.
- Zuur, A. F., Ieno, E. N., Walker, N. J., Saveliev, A. A., & Smith, G. M. (2009). Zero-Truncated and Zero-Inflated Models for Count Data. In A. F. Zuur, E. N. Ieno, N. Walker, A. A. Saveliev, & G. M. Smith (Eds.), *Mixed effects models and extensions in ecology with R* (pp. 261–293). Springer. https://doi.org/10.1007/978-0-387-87458-6_11

Supplemental Information

Contents

This supplemental Information document contains the following sections:

- 1) Motivating the DML plug-in estimator
- 2) Data Description
- 3) Abundance Ensemble Model
- 4) eBird Simulation
 - a. Generative Model
 - b. Simulation Scenarios
 - c. The Discrete-time stochastic exponential growth rate model
- 5) Directional Error
- 6) Simulation figures for Canada warbler and long-billed curlew
- 7) References for Supplemental Information

Section S1: Motivating the DML estimator

In this supplement we motivate the derivation of the plug-in estimator used in Double Machine Learning (Robinson, 1988). We begin with the outcome model (Equation (1) in the main text) that relates the abundance Y to the interannual trend τ and the effects of features X ,

$$Y = \tau \text{Year} + \mu(X) + \epsilon. \quad (\text{S1})$$

If we take the expectation of Equation (S1) over Year ,

$$E[Y] = \tau E[\text{Year}] + \mu(X). \quad (\text{S2})$$

The propensity score model from Equation (2) in main text is

$$\text{Year} = s(X) + \delta,$$

where δ is a stochastic error term with $E[\delta|X] = 0$. Thus, $E[\text{Year}] = s(X)$, and substituting

$$E[Y] = \tau s(X) + \mu(X) = m(X). \quad (\text{S3})$$

The function $m(X)$ is the called the marginal model.

To get the plug-in estimator, we rewrite (S3) as

$$\mu(X) = m(X) - \tau s(X),$$

and substitute $\mu(X)$ into Equation (S1),

$$Y = m(X) - \tau s(X) + \tau \text{Year} + \epsilon.$$

Next, we rearrange the left side of the equation to isolate the change in abundance by regressing out the effects of features X on Y ,

$$(Y - m(X)) = -\tau s(X) + \tau \text{Year} + \epsilon$$

Finally, we rearrange the right side of the equation to remove the effects of confounding by regressing out the effects of features X on Year ,

$$(Y - m(X)) = \tau (\text{Year} - s(X)) + \epsilon. \quad (\text{S4})$$

This expression motivates the three-step fitting procedure where m and s are estimated separately, and then plugged into Equation S4 to estimate the trend, τ . Practically, the plug-in estimator is attractive because it is straightforward to implement. The marginal function $m(X)$ can be learned using responses Y and features X . In practice, this can be done by simply permuting Year or excluding it from the feature set to restrict the model from learning patterns of interannual variation. The propensity score model can also be learned using the data in hand, using Year as the outcome variable and features X .

The plug-in estimator in Equation (S4) was originally developed for use with unbiased estimators (i.e., linear models). However, if biased estimators are plugged in then Equation (S4) will also be biased. This limitation excludes all modern statistical and machine learning models that employ penalization or regularization, a large class of models including penalized regression, random effects

models, generalized additive models, models that use the lasso, boosted models, neural network-based models, etc.

Double machine learning solved this problem using a combination of orthogonality and sample-splitting to accurately estimate τ even when the plug-in estimates suffer from regularization bias. Moreover, statistical analysis of DML has established general regularity conditions for the asymptotic convergence and normality of the DML estimator (Chernozhukov et al., 2018) and specifically for the causal forest implementation used in this study (Wager & Athey, 2018). Thus, unlike many machine learning methods, DML can be used for statistical inference, and, with sufficient assumptions, for causal inference.

Section S2: Data description

In this supplement we provide a detailed description of the data and data processing, including the aggregation, used for the eBird analysis.

The bird observation data were obtained from the citizen science project, eBird (Sullivan et al., 2014). We used a subset of data in which the time, date, and location of each survey were reported, and observers recorded the number of individuals of all bird species detected and identified during the survey period, resulting in a 'complete checklist' of species on the survey (Sullivan et al., 2009). Only the first participant's checklist was considered on group checklists. We further restricted checklists to those collected with 'stationary' or 'traveling' protocols from January 1, 2007 to December 31, 2019 within the spatial extent between 25° and 55° north latitude and 137 and 50 west longitude. Traveling surveys were restricted to those ≤ 15 km. The resultant dataset consisted of 23,841,789 million checklists. Each species' trend analysis and simulations were based on a breeding season subset of this dataset based on the species-specific breeding season definitions. Breeding season dates were defined for each species as the dates within which the population was assumed to be stationary. For resident species we defined the breeding season as a contiguous period within the year when detectability was highest, providing the largest power for trend estimation. For migratory species we defined season dates delimiting the breeding seasons published in (Fink, Auer, Johnston, Strimas-Mackey, et al., 2020).

The observation effort variables were: (a) the duration spent searching for birds, (b) whether the observer was stationary or traveling, (c) the distance traveled during the search, (d) the number of people in the search party, and (e) the Checklist Calibration Index (CCI), a standardized measure indexing differences in behavior among observers and checklists (Kelling et al., 2015). Note, only the first observer's CCI was associated with checklists that contain more than one observer.

The temporal variables included observation time of the day, which was standardized across time zones and daylight savings times as the difference from solar noon, was used to model variation in availability for detection, e.g. variation in behavior such as participation in the dawn chorus (Diefenbach et al., 2007). The day of the year (1-366) on which the search was conducted was used to capture intra-annual variation and the year of the observation was included to account for inter-annual variation.

Spatial and spatiotemporal descriptors of the local environment were variables describing elevation, topography, shorelines, islands, land cover, land use, hydrology, and road density (Meijer et al., 2018). To account for the effects of elevation and topography, each checklist location was associated with elevation (Becker et al., 2009), eastness, and northness. These latter two topographic variables combine slope and aspect to provide a continuous measure describing geographic orientation in combination with slope at 1 km² resolution (Amatulli et al., 2018). Each checklist was also linked to a series of covariates derived from the NASA MODIS land cover, land use, and hydrology data; MCD12Q1 (Friedl & Sulla-Menashe, 2019). We selected this data product for its moderately high spatial resolution and annual temporal resolution to capture spatial patterns of

change in land cover, land use, and hydrology. We used the FAO-Land Cover Classification System which classifies each 500m pixel into land cover one of 21 vegetative cover classes, along with additional classifications describing the land use and hydrology of each pixel. Checklists were linked to the MODIS data by year from 2001-2018, capturing inter-annual changes in land cover. The checklist data for 2019 were matched to the 2018 data, as MODIS data from after 2018 were unavailable at the time of analysis. Additionally, to delineate the interface between terrestrial, aquatic, and marine environments we used NASA MODIS land water classification MOD44W (Carroll et al., 2017, p. 44) in conjunction with 30m shoreline and island data (Sayre et al., 2019) and the elevation data described above to classify each pixel into land, ocean, inland water, and coastal areas. Finally, to identify habitat for coastal species, tidal mudflats were classified in three-year windows (Murray et al., 2019).

Data Description	Class	Data Source
Longitude	NA	Sullivan et al. 2014
Latitude	NA	Sullivan et al. 2014
Year	NA	Sullivan et al. 2014
Day	NA	Sullivan et al. 2014
Solar Noon Time	NA	Sullivan et al. 2014
Search Effort Duration (hrs)	NA	Sullivan et al. 2014
Search Effort Distance (km)	NA	Sullivan et al. 2014
Number of Observers	NA	Sullivan et al. 2014
CCI	NA	Sullivan et al. 2014
Elevation (m)	NA	Becker et al. 2009
Eastness slope/aspect component	NA	Becker et al. 2009, Amatulli et al. 2018
Northness slope/aspect component	NA	Becker et al. 2009, Amatulli et al. 2018
Island indicator	NA	Sayre et al. (2018) (30)
Tidal Mudflats	NA	Murray et al. (2019) (31)
Ocean	NA	Carroll et al. 2017, Sayre et al. (2018)
River	NA	Carroll et al. 2017, Sayre et al. (2018)
Lakes	NA	Carroll et al. 2017, Sayre et al. (2018)
Barren	1	Friedl & Sulla-Menashe 2019
Permanent Snow and Ice	2	Friedl & Sulla-Menashe 2019
Evergreen Needleleaf Forests	11	Friedl & Sulla-Menashe 2019
Deciduous Broadleaf Forests	14	Friedl & Sulla-Menashe 2019
Mixed Broadleaf/Needleleaf Forests	15	Friedl & Sulla-Menashe 2019
Mixed Broadleaf Evergreen/Deciduous Forests	16	Friedl & Sulla-Menashe 2019
Open Forests	21	Friedl & Sulla-Menashe 2019
Sparse Forests	22	Friedl & Sulla-Menashe 2019
Dense Herbaceous	31	Friedl & Sulla-Menashe 2019
Sparse Herbaceous	32	Friedl & Sulla-Menashe 2019
Dense Shrublands	41	Friedl & Sulla-Menashe 2019
Shrubland/Grassland Mosaics	42	Friedl & Sulla-Menashe 2019
Sparse Shrublands	43	Friedl & Sulla-Menashe 2019
Forest/Cropland Mosaics	25	Friedl & Sulla-Menashe 2019
Natural Herbaceous/Croplands Mosaics	35	Friedl & Sulla-Menashe 2019
Herbaceous Croplands	36	Friedl & Sulla-Menashe 2019
Woody Wetlands	27	Friedl & Sulla-Menashe 2019
Herbaceous Wetlands	50	Friedl & Sulla-Menashe 2019
Tundra	51	Friedl & Sulla-Menashe 2019
Urban and Built-up Lands	9	Friedl & Sulla-Menashe 2019
Highways	NA	Meijer et al. 2018
Primary Roads	NA	Meijer et al. 2018
Secondary Roads	NA	Meijer et al. 2018
Tertiary Roads	NA	Meijer et al. 2018
Local Roads	NA	Meijer et al. 2018

Table SI-1 Variables used in trend analysis.

To prepare these data for the trend analysis we aggregated all checklists, separately for each year, using a spatio-temporal grid whose dimensions were (27km × 27km × 1week) based on the latitude, longitude, date, and year of each checklist. In each grid cell, counts of the given species were summed for all checklists within each grid cell. Grid cells without any detections of this species during any weeks during any years were removed. We aggregated all observation effort variables by summing to represent the total effort within each grid cell. Summing counts in this way strengthens abundance signals making it easier to detect trends among species that are detected less frequently and species with relatively low abundance.

We also calculated the mean search duration and distance within each grid cell. Grid cell CCI values were computed as the average CCI within each grid cell weighted by search duration. The grid cell mean values were calculated for the time of day when surveys were initiated and for the day of the year when surveys were conducted. To keep track of the survey year, we also created a new variable for each grid cell indicating the unique year when surveys were conducted within the cell.

All spatial and spatiotemporal variables were summarized within grid cells using two metrics. The first metric describes the mean or *composition* of the variable across the grid cell landscape. The second metric describes the variation or *spatial configuration* of the variable across the grid cell landscape. For the categorical class variables, we computed the composition as the proportion of each class within each grid cell (PLAND) and we computed the spatial configuration using an index of its edge density within each grid cell (ED) using the R package *landscapemetrics* (Hesselbarth et al., 2019; McGarigal et al., 2012) . For the continuous variables (elevation, eastness, and northness) we computed the median and standard deviations for the composition and configuration, respectively.

SECTION S-3: The Abundance Ensemble

The ensemble was generated by refitting the causal forests with training datasets randomized to capture sampling variation and variation arising from the randomized spatiotemporal aggregation procedure. First, 75% of the available checklists we randomly sampled. Second, we aggregate the sampled checklists using a randomly located grid. To generate additional independence between the occurrence and count stages of the hurdle model, the training data were independently sampled and aggregated for the occurrence and count model training. We computed 25 ensemble estimates each for the occurrence and count models. To estimate trends in population abundance and their uncertainty we considered the ensemble consisting of all 625 unique combinations of occurrence and count estimates. We did not choose to compute more ensemble members because of the high computational cost of computing ensemble estimates for the simulation analyses.

Section S-4: eBird Simulation

In this supplement we provide additional details about the generative model, the simulation scenarios, and the discrete-time stochastic growth rate model used in the eBird simulation.

Section S-4.1: The Generative model

The goal of the generative model was to train a model to predict expected patterns of species abundance based on user-specified population trends along with realistic ecological and observational patterns learned from data. To do this we used the Boosted Regression Trees (BRT) hurdle model described in Fink, Auer, Johnston, Ruiz-Gutierrez, et al., (2020).

Let $(N, Y, X_e, X_o, year)$ be the set of training data for a given region, season, and species where:

- N is the $n \times 1$ vector of observed counts on the n surveys in the training data,
- Y is the $n \times 1$ vector that indicates the checklists with count greater than zero,
- X_e is the $n \times k$ matrix of k predictors that describe the ecological process,
- X_o is the $n \times j$ matrix of j predictors that describe the observation process, and
- $year$ is the $n \times 1$ vector of the year each survey was conducted.

To begin, we present a BRT hurdle model for species abundance and then we explain the modifications used for the generative model. In the first step of the unmodified BRT hurdle model, a Bernoulli response BRT is trained to predict the probability of occurrence:

$$Y \sim \text{Bernoulli}(\pi)$$

$$\text{logit}(\pi) = f(X_e, X_o, \text{year})$$

where π is the probability of occurrence and the function $f()$ is fit using boosted decision trees. In the second step, the Poisson response BRT,

$$N \sim \text{Poisson}(\mu)$$

$$\text{log}(\mu) = f(X_e, X_o, \text{year})$$

is trained to predict the expected counts μ , using the subset of the training data observed to be occupied.

To generate simulated counts of reported birds we modify the BRT as follows. The first modification permutes the *year* predictor variable. This ensures that the BRTs cannot learn year-to-year variation from the training data. The second modification trains the hurdle BRT with an offset constructed to impart a user-specified trend when training the model. The modified fitting procedure begins with the Bernoulli response BRT, trained with the permuted year,

$$Y \sim \text{Bernoulli}(\pi)$$

$$\text{logit}(\pi) = f(X_e, X_o, \text{year}^p),$$

The Poisson response BRT is trained with the permuted year and the offset, O ,

$$N \sim \text{Poisson}(\mu)$$

$$\text{log}(\mu) + O = f(X_e, X_o, \text{year}^p).$$

The offset can be considered as an adjustment to the expected observed counts, on the log-link scale. We construct the offset $O = g(\text{year}^p)$ where $g()$ is a function of the permuted year value, year^p . Because the offset is the only source of interannual variation, with respect to year^p , it forces the boosting procedure to learn the user specified population trend.

Section S-4.2: The Simulation Scenarios

The three types of spatial trend offsets constructed were: 1) spatially constant trends, 2) spatially varying trends and 3) no trend. We used the following linear model to construct the trend offsets, $O = \alpha \text{year}^p + \alpha_I \text{year}^p X_I$, where α controls the strength and direction of the overall year-to-year changes in the expected log count and α_I controls the strength of the interaction between *year* and X_I , the interacting variable. Note that because an intercept is fit as part of $f()$, we do not include an intercept term in the offset.

Spatially uniform trends were generated by setting $\alpha_I = 0$. Trends that affect a population uniformly over a region may indicate the indirect effects of broad-spatial scale processes like climate change. Spatially varying trends can be generated by setting $\alpha = 0$ and specifying a spatially patterned variable X_I to interact with year^p . To assess if spatial patterns associated with density dependent population processes can be detected, the spatially interacting variable was selected to be the land cover composition feature with highest importance score from the occurrence model and that had sufficient detections of the focal species across a range of land cover values. In this way the interacting variable functions as an index of population density. Processes like habitat loss, disease, and dispersal can interact with population density to generate spatially varying trend patterns, e.g. (Massimino et al., 2015).

The spatially constant trend values were generated by using annual changes in the count part of the model on the log scale defined as values $\alpha = (-0.08, -0.04, 0.04, 0.08)$. The largest absolute values for the spatially constant trend (-0.08 and 0.08) were selected to generate spatially constant trends of approximately 6.7% per year averaged across species' ranges. With the spatially variable trends, positive and negative directions generated inversely related trend patterns, but both varying in association with the same landcover covariate (See Figure 2 in the main text and Figures SI-2 and

SI-3). The spatially varying trend values were generated with the parameter interacting with landcover varying across values $\alpha_l = (-0.40, -0.20, 0.20, 0.40)$, with the largest values selected to generate relatively large regions within the species' range experiencing changes in population size of at least 6.7% per year.

SECTION S-4.3: The Discrete-time stochastic exponential growth rate model

In this supplemental section we describe the discrete-time stochastic exponential growth rate model used to incorporate population dynamics and temporal correlation into the simulated data sets. To set notation, we begin with the deterministic discrete-time exponential growth model,

$$N_{t+1,s} = (1 + r_s)N_{t,s}$$

where

- $N_{t,s}$ is an index of population size at time t and location s . In this study, $N_{t,s}$ is the count of the species on the checklist indexed by year t and location s ,
- r_s is the growth rate at location s . In our simulations r_s is constant across years. We describe the rate of population change in terms of the *Percent Per Year (PPY)* change, so that $r_s = \text{PPY}/100$, and
- t indexes years $1 \dots T$ of the study period.

The stochastic growth rate model can be written as

$$N_{t+1,s} = R_{t,s}N_{t,s},$$

where $R_{t,s}$ is a random variable with $E(R_{t,s}) = (1 + r_s)$, the deterministic component of population growth, and $sd(R_{t,s})$, that captures the stochastic component of population growth.

To parameterize the model, it is convenient to take logarithms,

$$\ln N_{t+1,s} = \ln N_{t,s} + \ln R_{t,s}.$$

We let $\ln R_{t,s} \sim N(\mu_{R,s}, \sigma_R^2(s))$ and write

$$\ln N_{t+1,s} = \ln N_{t,s} + \mu_{R,s} + \epsilon_t(s),$$

Where $\mu_{R,s} = E[\ln R_{t,s}]$ and $\epsilon_t(s) \sim N(0, \sigma_R^2(s))$. Assuming that locations are indexed according to a spatial grid, the stochastic component of $R_{t,s}$ varies independently between spatial grid cells and between years. This process can represent environmental stochasticity like the year-to-year effects of extreme weather on reproductive success. Populations within the same grid cell experience the same environmental conditions affecting population growth. Despite the year-to-year independence of the stochastic effects, the population trajectories generated by this process will be temporally correlated within each grid cell due to the compounded effects of the stochasticity across years.

To generate realizations from the discrete-time stochastic exponential growth rate model two parameters need to be specified: r_s describing the deterministic component of population growth and $\sigma_R(s)$ describing the stochastic component of population growth. For each simulation scenario, the values of r_s are constructed from the generative model. To specify $\sigma_R(s)$ consider the following relationship between parameters of the normal and lognormal distributions,

$$sd(R_{t,s}) = E(R_{t,s}) \sqrt{(\exp(\sigma_R^2(s)) - 1)}.$$

Because $r_s = \frac{\text{PPY}}{100}$, the range of values in which we are interested is relatively small, i.e. closer to 0.0 than to 1.0 in magnitude. For example, consider the 6.7 and 3.2 percent per year values used as IUCN RedList criteria (IUCN, 2019) and in the simulations. It follows that the standard deviation of r_s will likely be small, i.e. closer to 0.0 than to 1.0. Using the fact that these values are assumed to be

small, and that $R_{t,s} = 1 + r_s$, we know that $E(R_{t,s}) \approx 1$, $\sqrt{(\exp(\sigma_R^2(s)) - 1)} \approx \sigma_R(s)$ and that $sd(R_{t,s}) = sd(r_s)$. Using these facts and substituting into the expression for $sd(R_{t,s})$ yields $sd(R_{t,s}) = \sigma_R(s)$.

Thus, $100\sigma_R(s)$ is approximately the standard deviation in units of percent-per-year population growth.

For all simulation scenarios we specified $100\sigma_R(s)$ to be six percent per year. We chose this value to achieve a coefficient of variation for the growth rate of approximately 1 for the strong magnitude simulation scenarios and a coefficient of variation less than one for moderate and weak scenarios.

SECTION S-5 Directional Error

In this supplemental section we describe how we assessed estimates of the trend direction (increasing or decreasing). Directional errors were defined to occur when non-zero trends estimated the direction incorrectly. Non-zero trends were defined to occur when the 80% confidence interval did not contain zero. Filtering out non-zero locations was an important step because estimating trends with sparse, noisy data is a difficult estimation task. This can be seen from the size of the uncertainty estimates (Figure 3 in the main text).

Like many classification tasks, we expected that the ability to detect non-zero trends (a measure of power) and the ability to avoid directional errors (false positive errors) would vary with the magnitude of the trend, reflecting the underlying signal-to-noise ratio. Understanding the associations between power and error rates and trend magnitude is useful for interpreting simulation performance and generalizing to the analysis of real data. To do this we summarized the proportion of interval estimates overlapping zero and the proportion of directional errors as a function of estimated trend magnitude, binned into half percent increments. This summarization was carried out across all 27km locations for 10 realizations from each of the 5 simulation scenarios held aside for model assessment.

Figure SI-1 shows how the power to detect non-zero trends increases rapidly with trend magnitude and the directional error rate decreases with trend magnitude across all simulations for all three species.

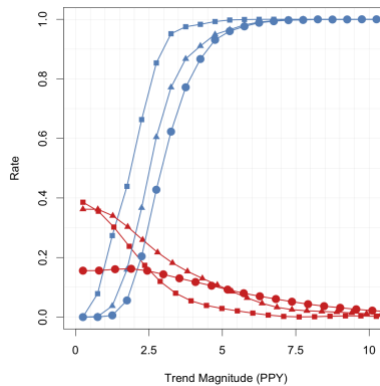


Figure SI-1 Power detecting non-zero trends and directional error rates as functions of trend magnitude. Blue lines show the power to detect non-zero trends as a function of trend magnitude binned into half Percent Per Year (PPY) increments for wood thrush (squares), Canada warbler (triangles), and long-billed curlew (circles). Red lines show the directional error rate as a function of trend magnitude binned into half Percent Per Year (PPY).

To summarize the species-level directional error rate across simulations we chose to report the mean directional error rate, averaged by magnitude binned into half-degree increments (Table 2 in main text). Implicitly, this measure gives each magnitude bin equal importance. This is a useful property when comparing analyses because it avoids confounding differences in the distribution of simulated trend magnitudes with the difference in error rates we are interested in.

SECTION SI-6 Simulation Results for Canada warbler and long-billed curlew

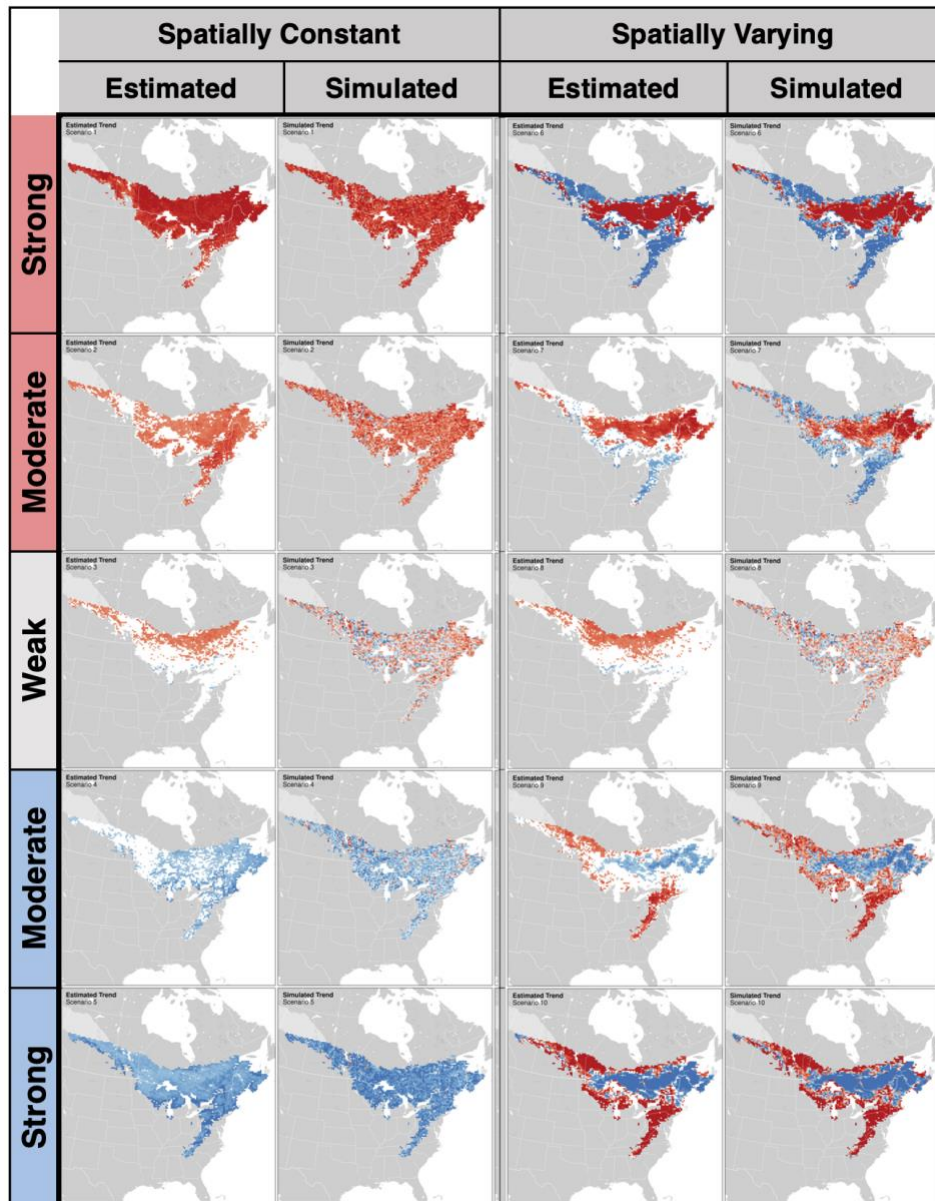


Figure SI-2: Canada Warbler Trend Simulations. All trend maps show the average annual percent-per-year change in abundance from 2007–2019 within 27km pixels (red=decline, blue=increase, white=non-significantly different from 0 at $\alpha = 0.2$), intensity (darker colors indicate stronger trends). Simulated trends show scenarios varying by direction and magnitude along rows: weak (includes trends $\sim |1\%/yr|$), moderate (includes regions with trends $\sim |3.5\%/yr|$), and strong trends (includes regions with trends $\sim |6.7\%/yr|$). The columns show simulated and estimated trends for spatially constant and varying simulation scenarios.

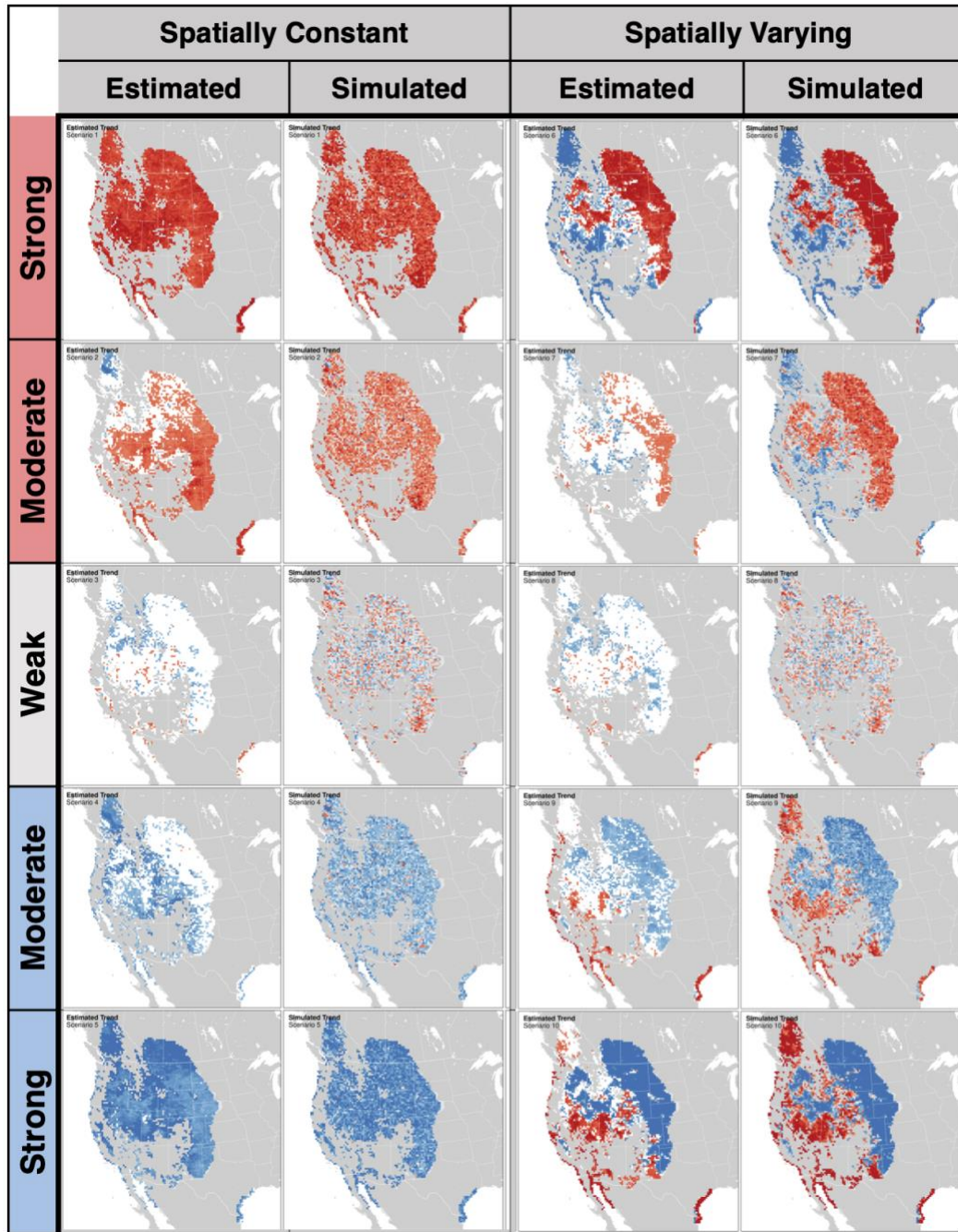


Figure SI-3: Long-Billed Curlew Trend Simulations. All trend maps show the average annual percent-per-year change in abundance from 2007–2019 within 27km pixels (red=decline, blue=increase, white=non-significantly different from 0 at $\alpha = 0.2$), intensity (darker colors indicate stronger trends). Simulated trends show scenarios varying by direction and magnitude along rows: weak (includes trends $\sim |1\%/yr|$), moderate (includes regions with trends $\sim |3.5\%/yr|$), and strong trends (includes regions with trends $\sim |6.7\%/yr|$). The columns show simulated and estimated trends for spatially constant and varying simulation scenarios.

Section SI 7: References for Supplemental Information

- Amatulli, G., Domisch, S., Tuanmu, M.-N., Parmentier, B., Ranipeta, A., Malczyk, J., & Jetz, W. (2018). A suite of global, cross-scale topographic variables for environmental and biodiversity modeling. *Scientific Data*, 5(1), Article 1. <https://doi.org/10.1038/sdata.2018.40>
- Becker, J. J., Sandwell, D. T., Smith, W. H. F., Braud, J., Binder, B., Depner, J., Fabre, D., Factor, J., Ingalls, S., Kim, S.-H., Ladner, R., Marks, K., Nelson, S., Pharaoh, A., Trimmer, R., Von Rosenberg, J., Wallace, G., & Weatherall, P. (2009). Global Bathymetry and Elevation Data at 30 Arc Seconds Resolution: SRTM30_PLUS. *Marine Geodesy*, 32(4), 355–371. <https://doi.org/10.1080/01490410903297766>
- Carroll, M., DiMiceli, C., Wooten, M., Hubbard, A., Sohlberg, R., & Townshend, J. (2017). MOD44W MODIS/Terra Land Water Mask Derived from MODIS and SRTM L3 Global 250m SIN Grid V006 [Data set]. *NASA EOSDIS Land Processes DAAC*.
- Chernozhukov, V., Chetverikov, D., Demirer, M., Duflo, E., Hansen, C., Newey, W., & Robins, J. (2018). *Double/debiased machine learning for treatment and structural parameters*.
- Diefenbach, D. R., Marshall, M. R., Mattice, J. A., & Brauning, D. W. (2007). Incorporating Availability for Detection in Estimates of Bird Abundance. *The Auk*, 124(1), 96–106. <https://doi.org/10.1093/auk/124.1.96>
- Fink, D., Auer, T., Johnston, A., Ruiz-Gutierrez, V., Hochachka, W. M., & Kelling, S. (2020). Modeling avian full annual cycle distribution and population trends with citizen science data. *Ecological Applications*, 30(3), e02056.
- Fink, D., Auer, T., Johnston, A., Strimas-Mackey, M., Robinson, O., Ligocki, S., Hochachka, W., Wood, C., Davies, I., & Iliff, M. (2020). *EBird Status and Trends, Data Version: 2019; Released: 2020. Cornell Lab of Ornithology, Ithaca, New York*.
- Friedl, M., & Sulla-Menashe, D. (2019). *MCD12Q1 MODIS/Terra+ Aqua Land Cover Type Yearly L3 Global 500m SIN Grid V006. 2019, distributed by NASA EOSDIS Land Processes DAAC*.
- Hesselbarth, M. H., Sciaini, M., With, K. A., Wiegand, K., & Nowosad, J. (2019). landscapemetrics: An open-source R tool to calculate landscape metrics. *Ecography*, 42(10), 1648–1657.
- IUCN. (2019). *The IUCN Red List of Threatened Species. Version 2019*. <https://www.iucnredlist.org>
- Kelling, S., Johnston, A., Hochachka, W. M., Iliff, M., Fink, D., Gerbracht, J., Lagoze, C., Sorte, F. A. L., Moore, T., Wiggins, A., Wong, W.-K., Wood, C., & Yu, J. (2015). Can Observation Skills of Citizen Scientists Be Estimated Using Species Accumulation Curves? *PLOS ONE*, 10(10), e0139600. <https://doi.org/10.1371/journal.pone.0139600>
- Massimino, D., Johnston, A., & Pearce-Higgins, J. W. (2015). The geographical range of British birds expands during 15 years of warming. *Bird Study*, 62(4), 523–534.
- McGarigal, K., Cushman, S. A., & Ene, E. (2012). FRAGSTATS v4: Spatial pattern analysis program for categorical and continuous maps. *Computer Software Program Produced by the Authors at the University of Massachusetts, Amherst*. <http://www.umass.edu/Landeco/Research/Fragstats/Fragstats.html>, 15.
- Meijer, J. R., Huijbregts, M. A. J., Schotten, K. C. G. J., & Schipper, A. M. (2018). Global patterns of current and future road infrastructure. *Environmental Research Letters*, 13(6), 064006. <https://doi.org/10.1088/1748-9326/aabd42>
- Murray, N. J., Phinn, S. R., DeWitt, M., Ferrari, R., Johnston, R., Lyons, M. B., Clinton, N., Thau, D., & Fuller, R. A. (2019). The global distribution and trajectory of tidal flats. *Nature*, 565(7738), 222–225.
- Robinson, P. M. (1988). Root-N-consistent semiparametric regression. *Econometrica: Journal of the Econometric Society*, 931–954.
- Sayre, R., Noble, S., Hamann, S., Smith, R., Wright, D., Breyer, S., Butler, K., Van Graafeiland, K., Frye, C., & Karagulle, D. (2019). A new 30 meter resolution global shoreline vector and associated global islands database for the development of standardized ecological coastal units. *Journal of Operational Oceanography*, 12(sup2), S47–S56.
- Sullivan, B. L., Aycrigg, J. L., Barry, J. H., Bonney, R. E., Bruns, N., Cooper, C. B., Damoulas, T., Dhondt, A. A., Dietterich, T., & Farnsworth, A. (2014). The eBird enterprise: An integrated

- approach to development and application of citizen science. *Biological Conservation*, 169, 31–40.
- Sullivan, B. L., Wood, C. L., Iliff, M. J., Bonney, R. E., Fink, D., & Kelling, S. (2009). eBird: A citizen-based bird observation network in the biological sciences. *Biological Conservation*, 142(10), 2282–2292.
- Wager, S., & Athey, S. (2018). Estimation and inference of heterogeneous treatment effects using random forests. *Journal of the American Statistical Association*, 113(523), 1228–1242.